Since January 2020 Elsevier has created a COVID-19 resource centre with free information in English and Mandarin on the novel coronavirus COVID-19. The COVID-19 resource centre is hosted on Elsevier Connect, the company's public news and information website.

Virus Research 154 (2010) 86–97

Contents lists available at ScienceDirect

Virus Research

journal homepage: www.elsevier.com/locate/virusres

Review

The structural biology of PRRSV

Terje Dokland*

Department of Microbiology, University of Alabama at Birmingham, Birmingham, AL, United States

ARTICLE INFO

Article history:
Available online 6 August 2010

Keywords:
Cryo-electron microscopy
Envelope protein
Nidovirus
Nucleocapsid
Virion
Structure

ABSTRACT

Porcine reproductive and respiratory syndrome virus (PRRSV) is an enveloped, positive-sense single-stranded RNA virus belonging to the *Arteriviridae* family. Arteriviruses and coronaviruses are grouped together in the order *Nidovirales*, based on similarities in genome organization and expression strategy. Over the past decade, crystal structures of several viral proteins, electron microscopic studies of the virion, as well as biochemical and *in vivo* studies on protein–protein interactions have led to a greatly increased understanding of PRRSV structural biology. At this point, crystal structures are available for the viral proteases NSP1α, NSP1β and NSP4 and the nucleocapsid protein, N. The NSP1α and NSP1β structures have revealed additional non-protease domains that may be involved in modulation of host functions. The N protein forms a dimer with a novel fold so far only seen in PRRSV and other nidoviruses. Cryo-electron tomographic studies have shown the three-dimensional organization of the PRRSV virion and suggest that the viral nucleocapsid has an asymmetric, linear arrangement, rather than the isometric core previously described. Together, these studies have revealed a closer structural relationship between arteri- and coronaviruses than previously anticipated.

Contents

1. Introduction 86
2. Non-structural proteins 87
3. The major envelope proteins, M and GP5 89
4. The minor envelope proteins 89
5. Virus entry 90
6. The nucleocapsid protein 90
7. PRRSV virion structure 92
8. Organization of the nucleocapsid 93
9. Perspectives 94
Acknowledgments 94
References 94

1. Introduction

Porcine reproductive and respiratory syndrome virus (PRRSV) emerged in Europe and in the US in the early 1990s and has since become a problem to the swine industry worldwide. PRRSV causes a persistent and sometimes severe disease that is characterized by respiratory problems, weight loss and poor growth performance, as well as reproductive failure in pregnant sows (Rossow, 1998; Zimmerman et al., 1997). Measures to regulate the disease have been complicated by the pattern of persistent, subclinical infection with occasional epidemic outbreaks as well as the high heterogeneity of the virus and the failure of the antibody response to completely protect against viral re-infection and re-emergence (Batista et al., 2004; Blaha, 2000; Meng, 2000; Murtaugh et al., 2002).

PRRSV is a member of the *Arteriviridae* family of enveloped viruses with positive-sense (+) RNA genomes that also includes lactate dehydrogenase-elevating virus (LDV) of mice, equine arteritis virus (EAV) and simian hemorrhagic fever virus (SHFV) (Plagemann and Moennig, 1992; Snijder and Meulenberg, 1998).

Abbreviations: EAV, equine arteritis virus; EM, electron microscopy; FMDV, food-and-mouth disease virus; GP, glycoprotein; LDV, lactate dehydrogenase-elevating virus; LV, Lelystad virus; MHV, murine hepatitis virus; NSP, non-structural protein; ORF, open reading frame; PRRSV, porcine reproductive and respiratory syndrome virus; SARS-CoV, severe acute respiratory syndrome coronavirus; SHFV, simian hemorrhagic fever virus; TM, transmembrane; VLP, virus-like particle.

* 845 19th St South, BBRB 311, Birmingham, AL 35242, United States.
Tel.: +1 205 996 4502; fax: +1 205 996 2667.
E-mail address: dokland@uab.edu.

0168-1702/$ – see front matter © 2010 Elsevier B.V. All rights reserved.
doi:10.1016/j.virusres.2010.07.029

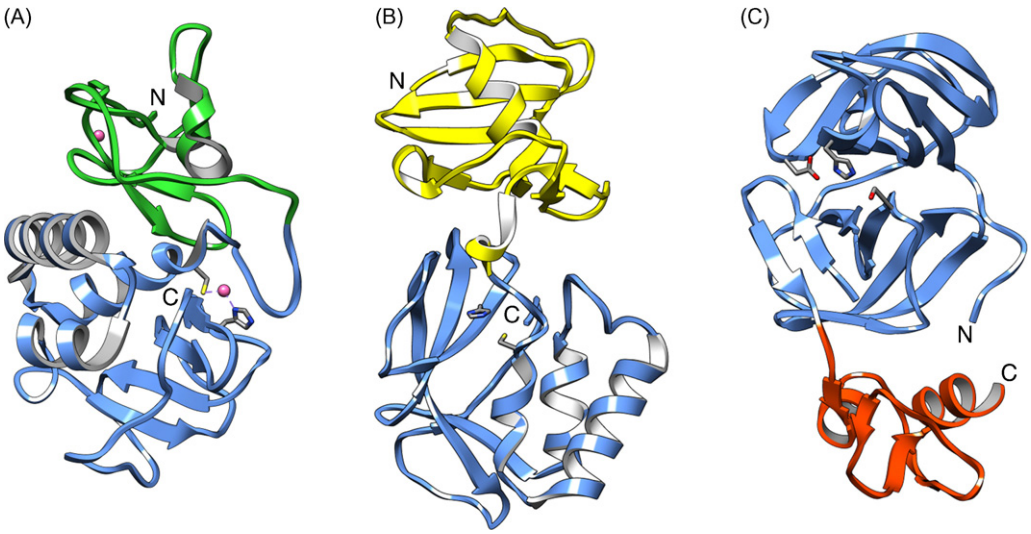

Fig. 1. Ribbon diagrams of the crystal structures of PRRSV NSP1α (A; PDB accession code 3IFU), NSP1β (B; 3MTV) and NSP4 (C; 3FAN) (Sun et al., 2009; Tian et al., 2009; Xue et al., 2010). In (A), the N-terminal zinc finger domain of NSP1α is colored green, the protease domain is blue. The active site residues Cys 76 and His 146 as well as the zinc finger Cys residues (Cys 8, Cys 20, Cys 25 and Cys 28) are shown in stick representation, and the two zinc ions are shown as pink balls. In (B), the N-terminal nuclease domain of NSP1β (including the linker between the two domains) is shown in yellow, while the protease domain is blue. The active site residues Cys 90 and His 159 are shown in stick representation. In (C), the chymotrypsin-like domain of NSP4 is blue, while the C-terminal domain is red. The active site residues His 39, Asp 64 and Ser 118 are shown as sticks. The figure was made with UCSF Chimera (Pettersen et al., 2004). (For interpretation of the references to color in this figure legend, the reader is referred to the web version of this article.)

PRRSV is divided into two genotypes, the European, or type 1 virus, also known as Lelystad virus (LV), and the American, or type 2 virus (Meng et al., 1995a). There is considerable sequence variability within both groups and only about 50–60% sequence identity between the two subtypes (Allende et al., 1999; Fang et al., 2007; Forsberg, 2005; Nelsen et al., 1999). Both subtypes now have a worldwide distribution (Fang et al., 2007; Gao et al., 2004; Nam et al., 2009; Ropp et al., 2004; Stadejek et al., 2002).

Based primarily on similarities in genome organization and transcription strategy, the arteriviruses are grouped together with coronaviruses, toroviruses and roniviruses in the order *Nidovirales* (Cavanagh, 1997; Snijder et al., 1993). Like in coronaviruses, the 15.1–15.5 kb PRRSV genome is expressed through a set of subgenomic mRNA transcripts (mRNA1–mRNA7), each used for the translation of one or two open reading frames (ORFs) (Conzelmann et al., 1993).

The full-length viral RNA (mRNA1) is used for the translation of two open reading frames, ORF1a and ORF1b. Translation of ORF1a yields the pp1a polyprotein. ORF1b is expressed through a ribosomal frame shift, leading to the formation of a large pp1ab polyprotein (den Boon et al., 1995; Meulenberg et al., 1993). The pp1a and pp1ab polyproteins are processed by viral proteases to release 14 non-structural proteins, which include four proteases (NSP1α, NSP1β, NSP2 and NSP4), the RNA-dependent RNA polymerase (NSP9), a helicase (NSP10) and an endonuclease (NSP11) (den Boon et al., 1995; Snijder and Meulenberg, 1998; van Aken et al., 2006; Ziebuhr et al., 2000).

ORFs 2–5 encode glycosylated membrane proteins GP2–GP5, ORF6 encodes a non-glycosylated membrane protein (M), and ORF7 encodes the nucleocapsid (N) protein (Dea et al., 2000; Meulenberg et al., 1995b; Snijder and Meulenberg, 1998). ORF2b is enclosed fully within ORF2 and encodes the small, non-glycosylated E or 2b protein (Wu et al., 2001). (Note that in some of the older literature, GP5 is also referred to as E, but this usage is no longer common.) The large number of envelope proteins is characteristic of nidoviruses, and all structural proteins were shown to be essential for infectivity (Molenkamp et al., 2000; Wissink et al., 2005).

It is noteworthy that the coronavirus genome follows much the same organization as the arteriviruses in spite of their much larger size (>30 kb). Some coronaviruses encode a few more ORFs, but mostly, the large size difference is taken up by encoding proteins of much larger size (Gorbalenya et al., 2006). In this sense, the arterivirus genome could perhaps be thought of as a "minimalist" nidovirus genome, while coronavirus represents an arterivirus genome with additional embellishments.

Until recently, little was known about the structure of the PRRSV virion and its component proteins. Early negative stain and thin section electron microscopy studies had revealed roughly spherical or oval particles of 60 nm diameter and a smooth external appearance (Dea et al., 1995; Horzinek, 1981; Mardassi et al., 1994). Occasionally, a 20–30 nm diameter core could be discerned, but no further structural details could be established from these studies. Recently, structures of the virion and some of the viral proteins, obtained by electron microscopy (EM) and X-ray crystallography, as well as *in vitro* and *in vivo* studies of protein–protein interactions have led to an improved understanding of PRRSV structure, assembly and infection process and shed light on the structural relationships between different nidoviruses.

This review will focus on the structural biology of PRRSV, i.e. the relationship between protein and virion structure and function, and how structural characteristics define the proteins' functional properties in the life cycle of the virus. Although I will take a broad view in what constitutes "structural" information, an emphasis will be placed on the recent protein and virus structures obtained by EM and crystallography as well as what can be gleaned from inspection of the protein sequences. When relevant, parallels between PRRSV and other systems will be drawn, in particular the relationship between PRRSV and other nidoviruses.

2. Non-structural proteins

Polyproteins pp1a and pp1ab are cleaved in a specific sequence by proteases encoded within ORF1a (de Vries et al., 1997; den Boon et al., 1995; Snijder and Meulenberg, 1998; Ziebuhr et al., 2000). At the N-terminus of pp1a are the two proteins NSP1α and NSP1β, which each includes a papain-like cysteine protease domain, called PCPα and PCPβ, respectively. NSP1α and NSP1β cleave themselves from the polyprotein at their C-terminal junctions (den Boon et al.,

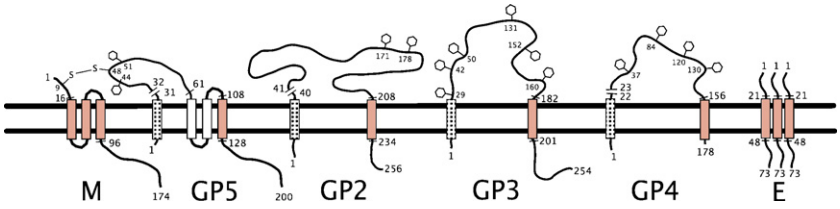

Fig. 2. Topology of PRRSV envelope proteins. Residue numbering is according to VR-2332 (a type 1 strain). Transmembrane domains are shown as rectangles crossing the lipid bilayer. The stippled boxes represent predicted signal peptides; the cleavage site is indicated by the broken line. (The GP3 signal peptide may not get cleaved.) Glycosylation is indicated by hexagons with the corresponding residues numbered. The disulfide link between M and GP5 is also indicated. E forms homo-oligomers and is shown as a trimer, but the exact number is not known.

1995; Ropp et al., 2004). Interestingly, NSP1α also appears to play a role in transcription (Kroese et al., 2008) and in EAV, NSP1 was found to co-localize with N in the nucleus of infected cells where it interacted with cellular transcription factors (Tijms et al., 2007; Tijms and Snijder, 2003).

Expression of an NSP1α/β fusion protein in *Escherichia coli* led to autocatalytic cleavage at the NSP1α/β junction, which occurred after Met 180 in PRRSV XH-GD, a type 2 strain, equivalent to His 180 in LV (Sun et al., 2009). The structure of NSP1α released upon such autocatalytic cleavage was determined crystallographically (Sun et al., 2009). The 180-residue protein exists as a dimer in solution and in the crystal. NSP1α contains an N-terminal zinc finger domain (residue 1–55), followed by a papain-like protease domain (PCPα, 66–166) and a short C-terminal extension (Fig. 1A). The zinc finger is a common motif in transcription factors, and may be responsible for the observed role of NSP1 in arterivirus RNA synthesis (Kroese et al., 2008; Tijms et al., 2007, 2001; Tijms and Snijder, 2003). The protease domain has a typical papain-like fold with similarities to papain-like proteases from other viruses, including FMDV L^{pro} (Guarne et al., 1998). The active site is comprised of Cys 76 and His 146 and is stabilized by a zinc ion in the crystal (Sun et al., 2009). The C-terminal extension was bound to the active site in the crystal, where it forms the substrate for its own protease activity. The release of NSP1α from the polyprotein thus enables subsequent processing by NSP1β (den Boon et al., 1995; Ziebuhr et al., 2000). In EAV, PCPα is not functional, due to a mutation of the active site Cys residue, and thus NSP1 is not cleaved into two separate entities (den Boon et al., 1995).

More recently, the structure of PRRSV NSP1β was also solved crystallographically (Xue et al., 2010) (Fig. 1B). The N-terminal part of NSP1β (residues 1–49) comprises a nuclease domain with activity on ssRNA and dsDNA. Residues 85–181 comprise a papain-like protease domain (PCPβ) that cleaves NSP1β from NSP2 autocatalytically after Gly 203. The protease active site is formed by Cys 90 and His 159 (Cys 96 and His 165 in LV) (den Boon et al., 1995; Xue et al., 2010). NSP1β forms dimers both in solution and in the crystals through contacts between its nuclease domains.

NSP2 is a large protein, varying in size from 1168 to 1196 residues between different PRRSV strains (Allende et al., 1999; Fang et al., 2004; Nelsen et al., 1999; Ropp et al., 2004). It is the most variable non-structural protein, with only 32% identity between subtypes (Allende et al., 1999). (By comparison, NSP2 of EAV is considerably smaller, with only 571 residues.) NSP2 contains a papain-like protease domain (PL2) near its N-terminus (residues 47–147), followed by a hypervariable region that is rich in prolines, a hydrophobic region containing four predicted TM helices, and a conserved C-terminal domain (Han et al., 2009). The PL2 protease activity is responsible for cleavage at the NSP2–3 junction (Han et al., 2009; Snijder et al., 1995). Residues Cys 55, Asp 89 and His 124 form the active site catalytic triad (Han et al., 2009). PL2 has deubiquitinating activity (Frias-Staheli et al., 2007) and may be equivalent to the papain-like protease domain (PLpro) of SARS-coronavirus, which is embedded in the NSP3 protein and acts as a deubiquitinase (Ratia et al., 2006). The cleavage specificity of the two proteins is similar, cleaving at GG pairs (Han et al., 2009). PRRSV PL2 is much smaller than the coronavirus protease and appears to be missing most of the β-sheet (the "fingers" domain) of PLpro, retaining the active site formed between helix α4 and the β-sheet in the "palm" domain (Ratia et al., 2006). The N-terminal ubiquitin-like (Ub1) domain of SARS-CoV PLpro also appears to be missing from PRRSV PL2.

The function of the rest of this protein is unknown, but appears to be involved in the formation of replication complexes in specialized cellular structures known as double-layered membrane vesicles (DMVs) observed during EAV replication (Pedersen et al., 1999; Snijder et al., 2001). Expression of an EAV NSP2–3 polyprotein was sufficient to induce the formation of DMVs (Posthuma et al., 2008; Snijder et al., 2001), and it is expected that the same will be true for PRRSV.

NSP3 has four predicted TM helices, which also appear to play a role in the formation of replication complexes and in anchoring other non-structural proteins in replication complex membranes (Han et al., 2009; Posthuma et al., 2008).

The remaining cleavages in both pp1a and pp1ab are carried out by the viral "main" protease, the NSP4 protein (Snijder et al., 1996; van Dinten et al., 1999), which is activated upon cleavage by the NSP2 protease at the NSP2–3 junction (Ziebuhr et al., 2000). The structures of NSP4 from both PRRSV and EAV have been solved crystallographically (Barrette-Ng et al., 2002; Tian et al., 2009). The two proteins are 34% identical in sequence and have a very similar structure. The protease domain of NSP4, residues 1–153, has a canonical chymotrypsin-like fold consisting of two six-stranded antiparallel β-barrels (Fig. 1C). This fold is found in numerous RNA viruses, including coronaviruses, picornaviruses and alphaviruses, and is referred to as a 3C-like protease (3CLP) (Allaire et al., 1994; Choi et al., 1991; Snijder et al., 1996). The active site of PRRSV NSP4 is formed by residues Ser 118, His 39 and Asp 64, located in the cleft between the two β-barrel domains. (Other non-arteri nidoviruses use Cys instead of Ser in the active site, Snijder et al., 1996.) Residues 157–199 comprise a C-terminal extension domain of a mixed α/β structure. While this domain is also very similar between PRRSV and EAV, it is shifted by about 8 Å in PRRSV relative to EAV when the chymotrypsin domains are superimposed (Barrette-Ng et al., 2002; Tian et al., 2009), but the functional relevance, if any, of this shift is unknown.

The remaining cleavage products of pp1a, NSP5–8, are not well described and have currently unknown functions and structures. NSP7 contains an internal cleavage site and was shown to be cleaved into two proteins NSP7α and NSP7β in EAV (van Aken et al., 2006) and presumably also in PRRSV. The additional proteins contained within pp1ab (NSP9–11) are the most conserved proteins within the nidoviruses (Gorbalenya et al., 2006). NSP9 is the viral RNA-dependent polymerase (van Dinten et al., 1996), NSP10 is a helicase that contains a zinc finger motif (Bautista et al., 2002; Seybert et al., 2005, 2000), and NSP11 is a nidovirus-specific uridylate-specific endonuclease (NendoU) (Nedialkova et

al., 2009). While no structures are known for any of these proteins, they should be expected to exhibit canonical structural motifs found in corresponding proteins from other sources.

3. The major envelope proteins, M and GP5

The major components of the PRRSV envelope are GP5 and M, which together comprise at least half of the viral protein and form disulfide-linked heterodimers in the virus (Dea et al., 2000; Mardassi et al., 1996; Meulenberg et al., 1995b; Wissink et al., 2005). Deletion of either of these two ORFs from an infectious PRRSV clone led to a failure to produce viral particles, while deletion of the minor envelope proteins did not have an effect on viral production (Wissink et al., 2005). However, co-expression of GP5, M and N was insufficient to release VLPs into the culture medium in EAV, suggesting that other factors (NSPs or host proteins) are required for particle formation and release (Wieringa et al., 2004).

From sequence-based topology prediction (TMHMM and HMMTOP), the non-glycosylated 174 residue (173 for type 1) M protein contains a short 16-residue N-terminal ectodomain followed by three transmembrane (TM) segments and an 84-residue C-terminal endodomain (Fig. 2). It is the most highly conserved structural protein of PRRSV (Meng et al., 1995b) and is also 22% identical in sequence between PRRSV and EAV.

The glycosylated 200-residue (201 for type 1) GP5 protein is the most variable protein of PRRSV, with only 51–55% sequence identity between the European and American subtypes (Kapur et al., 1996; Murtaugh et al., 1995). Hypervariability in GP5 is likely responsible for the lack of immunological cross-reaction between viruses (Meng, 2000). Sequence analysis (SignalP 3.0) indicates that residues 1–31 constitute an N-terminal signal sequence, which is followed by a predicted ectodomain that is glycosylated on Asn 44 and Asn 51 (Asn 46 and Asn 53 in LV) (Meulenberg et al., 1995b; Wissink et al., 2004, 2003) (Fig. 2). Glycosylation of Asn 46 was strongly required for both assembly and infectivity in LV, whereas N53 glycosylation did not appear to be important (Wissink et al., 2004). M and GP5 are disulfide linked between Cys 9 of M and Cys 48 of GP5 (Cys 8 and Cys 50 in type 1 strains) (Dea et al., 2000; Mardassi et al., 1996; Wissink et al., 2005).

Residues 60–125 of GP5 comprise a hydrophobic region that includes either one or three transmembrane (TM) helices (Balasuriya and MacLachlan, 2004; Dea et al., 2000; Mardassi et al., 1996; Wissink et al., 2004, 2003). Analysis of the PRRSV type 2 GP5 protein by TMHMM and HMMTOP predicts clearly only the last TM helix, between residues 107 and 125 (Fig. 2). A possible second TM helix is predicted between 63 and 82 in type 2 and, more strongly, between 68 and 90 in type 1. However, a second TM helix in this location would place the glycosylation sites of the ectodomain on the inside of the virus, an implausible arrangement. In EAV, where the ectodomain is much larger (about 100 residues), three TM helices are clearly predicted, thereby leaving the ectodomain on the outside of the virus where it belongs. While the evidence is not conclusive, this comparison suggests that three TM helices are present in PRRSV as well. In this case, the PRRSV GP5 ectodomain is only about 30 residues long, which would explain the very smooth appearance of PRRSV virions by EM (see below).

Like M, GP5 has a large C-terminal endodomain, from around residues 130 to 200. The large endodomains of the major envelope proteins is a unique feature in the nidoviruses. In the alphaviruses, the 33-residue endodomain of envelope protein E2 was found to form specific interactions with the nucleocapsid (C) protein during virus budding (Owen and Kuhn, 1997), and a similar role could be envisioned for the endodomains of PRRSV M and/or GP5. However, no interactions between the M endodomain and N could be detected in an *in vitro* pull-down assay (unpublished results); thus, the significance of the large endodomains of M and GP5 remains obscure.

There is no direct structural information available for either GP5 or M, but they are unlikely to have a similar fold to those of the envelope proteins of the flavi- or alphaviruses, based on size, topology and secondary structure prediction. Preliminary structural analysis of the M endodomain (residues 93–174) by NMR and CD spectroscopy showed that it was disordered in solution and did not contain significant secondary structure (unpublished results).

The primary role of both M and GP5 is probably structural, e.g. in imposing curvature on the viral membrane during budding. However, GP5 may also be involved in initial interactions with the host cell and perhaps fusion with host membranes (see below) (Wissink et al., 2004, 2005, 2003).

4. The minor envelope proteins

The GP2 glycoprotein has 256/residues in type 2 (253 in type 1) viruses. GP2 contains a predicted N-terminal signal sequence between residues 1 and 40 (1–37 in type 1) followed by a roughly 168-residue ectodomain, a single TM helix and a 20-residue endodomain (Wissink et al., 2004) (Fig. 2). GP2 has two conserved glycosylation sites, at residues Asn 171 and Asn 178 in type 2, or Asn 173 and Asn 179 in type 1 viruses, but glycosylation was not required for infectivity (at least not in type 1 viruses) (Meulenberg et al., 1995b; Wissink et al., 2004).

The small E or 2b protein is expressed from ORF2b, which is fully embedded within ORF2a that encodes GP2 (also called GP2a) (Wu et al., 2001). The 2b designation is somewhat confusing, since in EAV, the equivalent ORF starts slightly before the start codon of the ORF encoding GP2 and the protein is therefore sometimes called 2a. (Note, however, that the term E was previously used for GP5.) E is a non-glycosylated, 70–73-residue minor envelope protein (Wu et al., 2001, 2005). The E protein of EAV was shown to be essential for EAV infectivity, but not for particle assembly (Snijder et al., 1999; Wieringa et al., 2004). E consists of a single predicted TM helix and is thought to form an oligomeric ion channel (Lee and Yoo, 2006)(Fig. 2). This protein is therefore most likely involved in the viral fusion and/or internalization process, by analogy with similar proteins found in many other viruses, such as the M2 protein of influenza virus (Pinto et al., 1992) or the 6K protein of alphaviruses (Melton et al., 2002). These proteins form proton channels that are required to lower the internal pH of the virus during fusion in the low pH endosomal compartment (Gonzalez and Carrasco, 2003).

The 254-residue (265 in type 1) GP3 protein is a minor component of the viral envelope and is the most heavily glycosylated envelope protein of PRRSV (Gonin et al., 1998; Wierenga et al., 2002). The topology of GP3 is unclear; predictions (SignalP) show a TM domain from residues 1–27 and a putative TM domain from 183–200 (Fig. 2). The overall sequence identity between the US and European subtypes is 58%, but the highest divergence is in the C-terminal 30–50 residues, where the European subtype has an additional 11 amino acid extension. The predicted ectodomain is about 70% identical between the two subtypes. (By comparison, the 163-residue GP3 protein of EAV has a much shorter, 46-residue predicted ectodomain.) The first TM helix is predicted to comprise a signal peptide in both PRRSV and EAV; however, studies in EAV have shown that this peptide is not cleaved off (Wierenga et al., 2002) suggesting that the protein is anchored in the membrane at both the N- and C-terminal ends.

GP3 contains 6 predicted glycosylation in the putative ectodomain, on residues 29, 42, 50, 131, 152 and 160 in type 2 (27, 42, 50, 130, 151 and 159 in type 1) (Fig. 2). (One site was also predicted in the endodomain, which is presumably not used if the topology prediction is correct.) Mass estimates by SDS-PAGE have

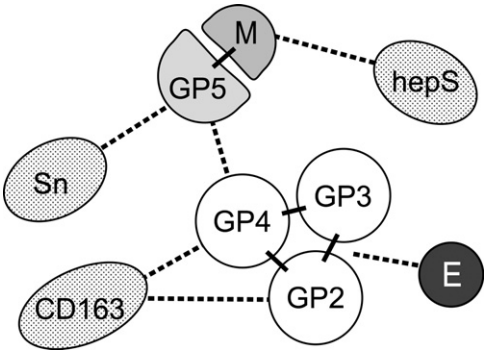

Fig. 3. Map of protein–protein interactions in the PRRSV envelope. The viral proteins are indicated as circles. Solid lines indicate the well-established, possibly covalent interactions that define the two major envelope protein complexes M–GP5 and GP2–GP3–GP4. Dashed lines indicate other (non-covalent) interactions. Interactions with the three host receptors proteins heparan sulfate (hepS), sialoadhesin (Sn) and CD163 are also shown. E interacts with the GP2–GP3–GP4 complex, but it is unclear which specific protein that is involved.

suggested that all six are used, adding as much as 16 kDa to its mass (Gonin et al., 1998), consistent with similar findings in EAV (Wierenga et al., 2002).

Some GP3 protein is secreted into the cell medium during PRRSV type 2 infections (Gonin et al., 1998; Mardassi et al., 1998; Wierenga et al., 2002) and it was initially thought not to be a structural protein. However, GP3 was subsequently identified as a minor component in both type 1 and 2 viruses (de Lima et al., 2009; van Nieuwstadt et al., 1996; Wissink et al., 2005). In PRRSV type 2, it was demonstrated by immuno-EM that GP3 is exposed on the viral surface (de Lima et al., 2009).

The GP4 minor envelope protein ranges in size from 178 (type 2) to 183 (type 1) residues (Meulenberg et al., 1997; van Nieuwstadt et al., 1996). GP4 contains a predicted cleaved signal peptide from residues 1 to 21, and most likely one TM helix at residues 156–177 (161–181 for type 1; Fig. 2). GP4 has four potential glycosylation sites at residues 37, 84, 120 and 130, at least three of which are likely to be used, by comparison with EAV, which lacks the fourth site (Wierenga et al., 2002).

GP2, GP3 and GP4 are incorporated as multimeric complexes in the envelopes of both type 1 and 2 viruses (Das et al., 2010; Wissink et al., 2005) (Fig. 3). At least in type 1 viruses, E is also part if this complex, and the lack of any of these four proteins led to a failure to incorporate the other three (Wissink et al., 2005). In EAV, the GP2–GP3–GP4 complex is disulfide linked (Wieringa et al., 2003a,b, 2004), but this has not been demonstrated for PRRSV. Immunoprecipitation studies have suggested that this complex interacts with GP5 via GP4 (Das et al., 2010)(Fig. 3). All proteins are required for infectivity (of type 1 viruses), but were not required for particle formation (Wissink et al., 2005). No direct structural information is yet available for any of the minor structural proteins.

5. Virus entry

PRRSV exhibits a strong tropism for differentiated porcine macrophages (Benfield et al., 1992; Duan et al., 1997; Kreutz, 1998), although growth in culture can also be done on the monkey kidney cell line MARC-145 (Kim et al., 1993). The most effective neutralizing antibodies to PRRSV were directed against GP5, suggesting that this protein may be the main determinant of protective immunity and might be involved in receptor binding (Gonin et al., 1999; Ostrowski et al., 2002; Pirzadeh and Dea, 1997; Weiland et al., 1999; Yang et al., 2000). However, GP5 does not appear to be responsible for defining tropism; swapping out the ectodomain of EAV GP5 with that of PRRSV or LDV did not affect the tropism of the virus (Dobbe et al., 2001). The same was also true for M (Verheije et al., 2002). Thus, cell tropism appears to be determined by a higher affinity binding of one or more of the minor envelope proteins to a cell-specific receptor protein (Wissink et al., 2004, 2005, 2003).

The first step in PRRSV infection of macrophages appears to be a low affinity attachment of the virus to heparan sulfate, apparently via the M-GP5 complex (Delputte et al., 2005, 2002) (Fig. 3). This step is not absolutely required for infection, but may concentrate the virus on the cell surface for subsequent binding to a higher affinity receptor.

Internalization, and hence the initiation of a productive infection, requires a higher affinity binding to the macrophage-specific sialic acid-binding protein (lectin) sialoadhesin (Siglec-1) (Delputte et al., 2005). This interaction is mediated via sialic acid present on GP5 (Delputte and Nauwynck, 2004; Van Breedam et al., 2010), which binds to the N-terminal immunoglobin domain on sialoadhesin (Delputte et al., 2007) (Fig. 3). MARC-145 cells do not have sialoadhesin, however, so in this case other factors are presumably used. Expression of sialoadhesin on PK-15 (porcine kidney) cells makes the cells able to internalize PRRSV, but does not lead to a productive infection (Vanderheijden et al., 2003). The virus in this case appears to be trapped in endosomes and fails to release the nucleocapsid into the cytoplasm.

Recent studies have shown that this final uncoating and release step is dependent on the scavenger receptor CD163 (Calvert et al., 2007). Expression of this protein in a number of cell types makes the cells susceptible to PRRSV infection (Calvert et al., 2007; Lee et al., 2010). Full susceptibility requires both sialoadhesin and CD163, however (Van Gorp et al., 2008). Immunoprecipitation studies of transfected cells indicated that CD163 interacts with GP2 and GP4 (Das et al., 2010) (Fig. 3).

In addition, successful infection is dependent on proteases that reside in the endosome, including cathepsin E and a yet unidentified serine protease (Misinzo et al., 2008). The role of the proteases is most likely to cleave and release the fusion peptide from the envelope proteins in order to initiate membrane fusion (Harrison, 2008). Similarly, fusion of coronaviruses SARS-CoV and MHV require the action of endosomal cathepsins B and L (Qiu et al., 2006; Simmons et al., 2005). The target for this activity in PRRSV and thus the identity of the protein containing the fusion peptide is still unknown. It could be speculated to reside in the predicted hydrophobic membrane-proximal regions of GP2, GP4 or GP5, which upon release by cleavage may form a membrane-insertion sequence.

6. The nucleocapsid protein

The 123–128 amino acid N protein interacts with the viral RNA to form the viral nucleocapsid. N is the product of ORF7, which is expressed from the smallest subgenomic mRNA (mRNA7), and is the most abundant viral protein expressed in infected cells (Dea et al., 2000; Meulenberg et al., 1995a). N is the most immunogenic viral protein, but anti-N antibodies are non-neutralizing and non-protective (Murtaugh et al., 2002).

The N protein is divided into an N-terminal RNA-binding domain and a C-terminal dimerization domain (Fig. 4A). The amino-terminal half of the N sequence (residues 1–57) is presumed to be mostly disordered and contains a large number of positive charges, consistent with a role in RNA binding (Yoo et al., 2003). The greatest sequence difference between PRRSV strains and with other arteriviruses is in this domain (Meng et al., 1995a), probably due to relaxed structural constraints.

A hydrophobic sequence within the N-terminal domain from residues 21 to 33 (25–37 in type 1 viruses) is predicted to form an α-helix (Fig. 4A). This characteristic is maintained between different arteriviruses in spite of low sequence conservation. Such a helix

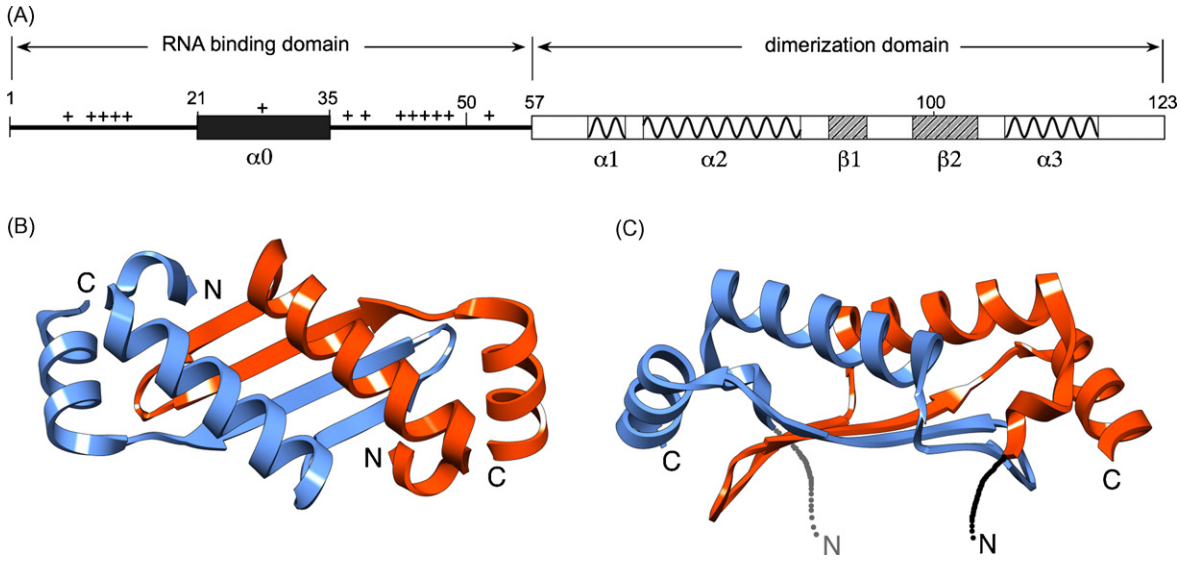

Fig. 4. Structure of the nucleocapsid protein. (A) Sequence of N, showing the division into an N-terminal RNA-binding domain (residues 1–57) and a C-terminal dimerization domain (58–123), represented by the NΔ57 construct. Secondary structure elements are shown, including the predicted hydrophobic helix (α0) in the RNA-binding domain. Positively charged residues in the RNA-binding domain are indicated by (+) signs. (B and C) Ribbon diagrams of the NΔ57 dimer (PDB accession code 1P65) in the "top" view (B), looking down on the two long α2-helices, and a "side" view (C), looking approximately perpendicular to the two α2-helices (Doan and Dokland, 2003). Positions of N and C termini and the extension of the N-terminal RNA-binding domains are indicated.

might play a role in assembly, for example through the formation of a coiled-coil structure with other N proteins. This is analogous to a similar α-helix found in the N-terminal RNA-binding domain of alphaviruses (Perera et al., 2001).

It was previously reported that N is incorporated into virions as disulphide-linked dimers (Mardassi et al., 1996; Wootton and Yoo, 2003). This dimerization was found to involve Cys 23 (equivalent to Cys 27 in type 1 viruses), which is within the N-terminal helix (Wootton and Yoo, 2003). In combination with non-covalent dimerization of the C-terminal domain (see below), such crosslinking of N proteins could provide a mechanism for particle assembly. However, other members of the *Arteriviridae* lack this Cys residue, indicating that disulfide linkage is not a requirement for assembly.

N is targeted to the nucleolus of infected cells by nuclear and nucleolar localization sequences within the RNA-binding domain (Rowland et al., 2003; Yoo et al., 2003). Furthermore, N was found to interact with a HIC (human I-mfa domain-containing protein) homologue, a zinc-binding transcriptional regulator (Song et al., 2009), suggesting that N may play a role in transcriptional regulation in PRRSV-infected cells. N is also phosphorylated on Ser residues in both the N- and C-terminal domains (Wootton et al., 2002). The functional significance of the phosphorylation is unclear, but it might play a role in the modulation of host functions.

The C-terminal half of the protein comprises a well-ordered dimerization or "capsid-forming" domain that forms dimers in solution. The crystal structure of this domain (NΔ57; residues 58–123) showed a dimer comprised of a four-stranded antiparallel β-sheet floor that is capped and flanked by α-helices (Doan and Dokland, 2003) (Fig. 4B and C). The crystal structure of the equivalent domain from the EAV N protein, comprising residues 49–110 (NΔ48), is essentially identical, with minor differences in some of the interspersing loops (Deshpande et al., 2007).

The PRRSV N protein dimerization domain represents the first discovered member of a fold so far only found in arteri- and coronavirus nucleocapsid proteins. Subsequent X-ray crystallographic and NMR structures of the C-terminal dimerization domains of the nucleocapsid protein from two coronaviruses, infectious bronchitis virus (IBV) and SARS-CoV, revealed a topologically equivalent fold (Chang et al., 2005; Chen et al., 2007; Jayaram et al., 2006; Yu et al., 2006). In the coronavirus N proteins, this 120–130-residue domain is embedded into a much larger nucleocapsid protein of 350–422 residues. This "nidovirus nucleocapsid fold" is different from the nucleocapsid structures of both flaviviruses (Dokland et al., 2004) and alphaviruses (Choi et al., 1997), showing that these three groups of (+) RNA viruses belong to distinct structural groups in spite of superficial structural similarities (Strauss and Strauss, 2002). The structural similarity between corona- and arteriviruses strongly suggests that these proteins evolved from a common ancestor, and reinforces the evolutionary relationships that are also reflected in their genome organization and replication strategy. In the coronaviruses, the much longer N-terminal RNA-binding domain also contains an ordered, β-rich domain that has been solved by NMR and X-ray crystallography (Fan et al., 2005; Huang et al., 2004; Jayaram et al., 2006). This domain has no equivalent in the arteriviruses.

The N protein fold is superficially similar to that of the coat protein of ssRNA bacteriophage MS2 (Valegård et al., 1990). The MS2 coat protein has a fold that is related to the human histocompatibility antigen (HLA) peptide-binding domain (Saper et al., 1991). However, the MS2 and HLA structures have more extensive, four-stranded β-sheets and their long α-helices sequentially succeed rather than precede the sheet. The two α2-helices of N would be equivalent to the helices that form the peptide-binding cleft in the HLA molecule and is exposed on the outside of the MS2 capsid. This superficial resemblance led to the suggestion that the PRRSV and EAV N proteins might be analogously organized into an icosahedral ($T = 3$) capsid with the α-helical cleft on the outside (Deshpande et al., 2007; Doan and Dokland, 2003). In the EAV-NΔ48 structure, the N dimers are organized into dimers of dimers, which seemed to support this idea (Deshpande et al., 2007).

In the PRRSV NΔ57 crystals, in contrast, the N dimers are arranged in parallel, undulating ribbons with a threefold helical twist, suggesting that the protein alternatively might take on a helical organization in the viral nucleocapsid (Doan and Dokland, 2003). This was further supported by the observation that full-length PRRSV N denatured in urea, followed by renaturation in the presence of tRNA formed long filamentous structures with an inter-fiber spacing of 4 nm, consistent with the crystal packing, in

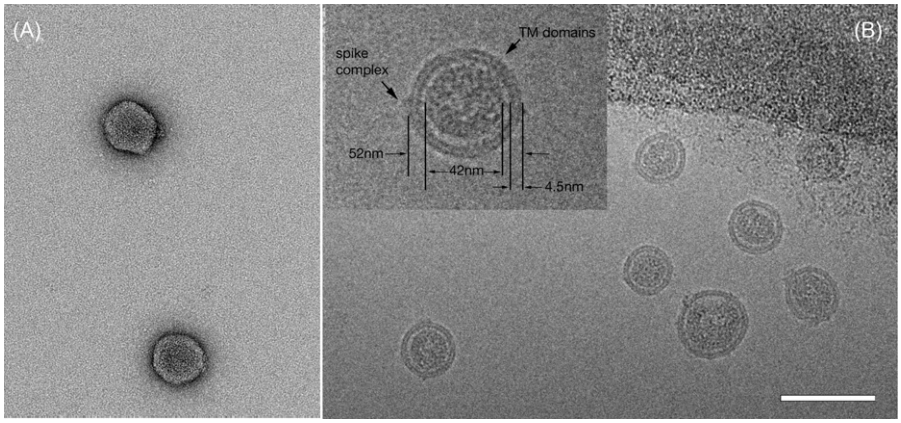

Fig. 5. Representative examples of PRRSV virions imaged by (A) negative stain EM (stained with 1% uranyl acetate) and (B) by cryo-EM. The inset in (B) shows one typical particle with pertinent dimensions indicated. Scale bar, 100 nm.

addition to shell-like structures of various sizes (Doan and Dokland, 2003). Similar results were found when a full-length EAV N protein was expressed as a maltose-binding protein (MBP), followed by removal of the MBP moiety (unpublished results).

Together these results suggest that the native conformation of the nucleocapsid in the virion may be helical and filamentous rather than the presumed icosahedral – or even isometric – shell. Indeed, this interpretation was supported by the subsequent cryo-EM and tomographic reconstruction of PRRSV (see below) and is also consistent with current models of coronavirus nucleocapsid structure (Barcena et al., 2009; Chen et al., 2007; Fan et al., 2005; Jayaram et al., 2006).

7. PRRSV virion structure

Earlier EM studies had shown the PRRSV virion as round or oval particles with a smooth outer appearance (Dea et al., 1995; Horzinek, 1981; Mardassi et al., 1994). Similar studies on other arteriviruses revealed similar features (Brinton, 1994; Horzinek, 1981; Snijder and Meulenberg, 1998). Limitations of the negative staining and plastic sectioning techniques used in these studies precluded the visualization of any further detail of PRRSV virion structure. Some studies showed a roughly isometric core, and it was generally assumed that the cores would be isometric and hence icosahedral, although there was no convincing evidence that this was the case. Coronaviruses have generally been described as pleiomorphic, roughly 100 nm diameter particles, with a "corona" of club-shaped protrusions representing the envelope proteins (Holmes and Lai, 1996).

By negative stain electron microscopy, PRRSV virions appears as roughly spherical to somewhat oval particles with a mean diameter of about 55 nm and a smooth, mostly featureless surface (Fig. 5A). No internal structures are discernable in intact particles by negative staining because of the inability of the stain to penetrate through the lipid envelope.

Cryo-EM allows the direct visualization of viruses and other specimens in their native, hydrated state, in the absence of staining and dehydration artifacts. By cryo-EM, PRRSV virions appear as round or egg-shaped particles ranging in diameter from 50 nm to 74 nm, with a median value of 54 nm and few particles larger than 60 nm (Fig. 5B). The particles display a very smooth outline with few protruding features, consistent with the small ectodomains of the major envelope proteins, M and GP5 (16 and 30 residues, respectively, corresponding to a feature of approximately 2 nm in size) (Mardassi et al., 1996; Meulenberg et al., 1995b). The lipid bilayer of the envelope is clearly discernible, and has a thickness of about 4.5 nm. This may include some contribution from the envelope protein endodomains, in particular M and GP5. For the MHV coronavirus, a thin layer corresponding to M endodomains could be distinguished from the inner leaflet of the lipid bilayer itself under appropriate imaging conditions, giving an apparent total membrane thickness of 7.8 nm (Barcena et al., 2009). In some places, the membrane has a set of cross-striations, which are assumed to correspond to envelope protein TM domains (Fig. 5B).

A few features protruding from the membrane surface by about 10–15 nm are also visible in the PRRSV images (Fig. 5B). These protrusions most likely stem from the more bulky, less abundant membrane proteins, such as GP2 (Wissink et al., 2005). The predicted GP2–GP3–GP4 heterotrimer would have 436 residues outside the membrane, roughly corresponding to a 5–10 nm structure, depending on its shape.

The virions contain an internal core with an average diameter of 39 nm, which is separated from the envelope by a 2–3 nm gap. The size and shape of the core generally follows that of the envelope and thus displays considerable variation. The core consists of a 10 nm thick layer of density surrounding a central, lower density area, suggesting that the core is hollow.

Except for the absence of the protruding spikes, the overall shape and organization of PRRSV observed by cryo-EM is not unlike that of coronaviruses (Barcena et al., 2009; Neuman et al., 2006a,b), suggesting that the structural and genetic relationships between corona- and arteriviruses also extend to the supramolecular organization of the virion.

Electron micrographs only represent a two-dimensional projection through the sample. Tomographic reconstruction uses information from multiple images at varying tilt angles to generate a three-dimensional representation of the sample. Tomography is a general procedure that does not depend on internal symmetry or the presence of multiple identical objects, although the resolution is limited by image noise and the missing wedge of information at high tilt angles (Lucic et al., 2005; Subramaniam, 2005). A single tomogram thus represents a 3D reconstruction of the entire field of view, which can then be sectioned computationally, thereby removing superimposing layers that obscure the features of interest.

Cryo-electron tomography reveals the pleiomorphic morphology of the PRRSV virions in greater detail and in three dimensions (Spilman et al., 2009). Fig. 6A shows a single, 15.8 Å thick section through part of one complete tomogram, which includes about 20 PRRSV particles with an average diameter of 56 nm. (Some differences in size and appearance of the particles results from the

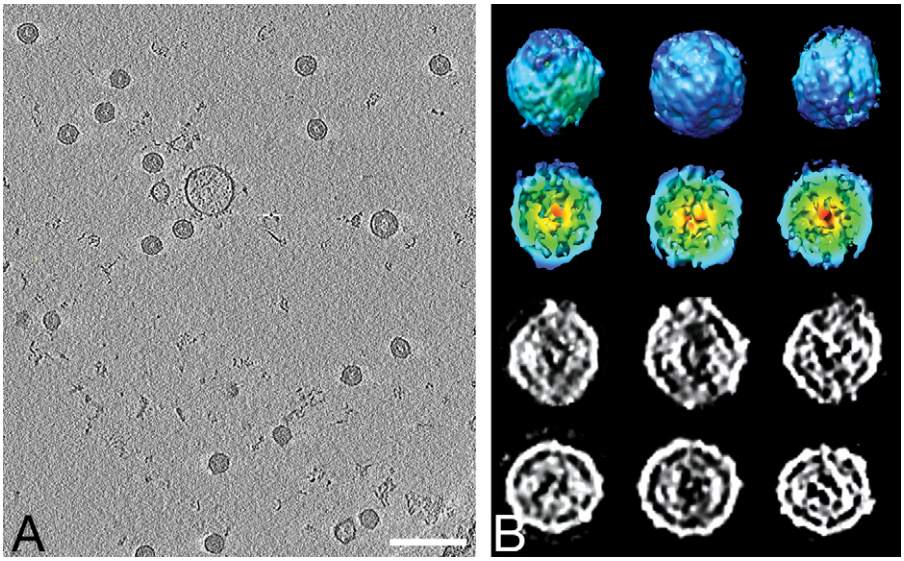

Fig. 6. Cryo-electron tomography of PRRSV. (A) Central section (15.8 Å thick) through one tomogram, showing numerous PRRSV virions. Scale bar, 200 nm. (B) Montage of individual PRRSV sub-tomograms. Each column represents a distinct particle in various representations, as follows: top row, isosurface of whole particle, viewed along *y*-axis ("side view"); second row, isosurface of half particle, colored from red to blue according to distance from the center; third row, central section through particles along *y*-axis ("side view", viewed perpendicular to the direction of the electron beam); bottom row, central section along *z*-axis ("top view", viewed parallel to the direction of the beam) (Spilman et al., 2009). (For interpretation of the references to color in this figure legend, the reader is referred to the web version of this article.)

different relative positions of each particle in the ice, and hence, in the place of the section.)

Individual particles were selected from the tomogram, filtered and masked to remove noise. Three representative particles are shown in Fig. 6B as isosurfaces (top and second rows) and central sections (third and last rows). The top three rows are viewed parallel to the plane of the ice and perpendicular to the direction of the beam, referred to as a "side view". The slightly drawn out appearance is an artifact caused by the "missing wedge" of information at high angles (Lucic et al., 2005; Subramaniam, 2005). The last row is a central section viewed parallel to the direction of the electron beam (along the *z*-axis, or a "top view"). In this view, the particles are more or less centrosymmetric (Fig. 6B).

As in the micrographs, the reconstructed PRRSV particles generally present a quite smooth and featureless outer surface (Fig. 6B). A few protruding features are evident on some of the particles, possibly corresponding to the bulkier minor envelope complexes. At the resolution of the tomogram, the two leaflets of the lipid bilayer, separated by about 3–4 nm, cannot be distinguished, consistent with observations in other tomographic reconstructions of viruses (Barcena et al., 2009; Harris et al., 2006). However, the internal core is clearly discerned as a double-layered, approximately 12 nm thick, hollow shell, separated from the envelope by a 3 nm gap that is traversed only by a few strands of density, possibly corresponding to envelope protein endodomains.

8. Organization of the nucleocapsid

In isosurface representation, the core looks disorganized and appears to consist of many strands of density bundled into a ball (Fig. 6B, second row). The tomograms typically have a single strong density in the center of the particles, which is connected to the rest of the core only on one side, perhaps corresponding to one end of the genome. In the central sections (Fig. 6B, third and bottom rows) it appears that each of the two layers of density in the core is comprised of a series of elongated densities of approximately 7 nm length, in many cases giving the appearance of a chain with a link-to-link distance of about 10 nm. One possible interpretation of this structure is that two layers of N dimers form a linked, twisted chain with the RNA in the middle, where it interacts with the N-terminal RNA-binding domains of N (Fig. 7). This chain is then bundled into a roughly spherical shape that leaves a hollow interior (Spilman et al., 2009).

The volume of the electron density enclosed by the core at a cutoff level of two standard deviations (2σ) above the mean corresponds to an average mass of 24.0 ± 2.9 MDa (25.5 ± 3.0 MDa at 1σ cutoff). After subtracting the mass of the genome (approximately 4753 kDa), this volume corresponds to 1415 copies of N in the core, consistent with theoretical considerations based on predicted RNA length and the model shown in Fig. 7 (Spilman et al., 2009).

While this organization is clearly incompatible with the idea of an isometric, icosahedrally symmetric core, it is not unlike nucleocapsid models suggested for coronaviruses. Although it is not known exactly how the coronavirus N protein is organized into a helical nucleocapsid (Davies et al., 1981; Sturman et al., 1980), several possible models have been proposed (Chen et al., 2007; Fan et al., 2005; Jayaram et al., 2006). In some of these models, the RNA forms the center of a helix made by the N proteins, while others have proposed that the RNA is wound around the outside of a helical N protein core. However, these models were based on high-resolution structures of nucleocapsid proteins that lack most of the RNA-binding domain and do not contain RNA. Recent cryo-electron tomographic structure determination of the MHV coronavirus suggests that the RNA–protein complex forms a helical coil, which in the micrographs gives rise to the appearance of a double-layered core similar to that observed for PRRSV (Barcena et al., 2009). While this interpretation would also be consistent with the PRRSV structure, the disordered appearance of the PRRSV core may suggest a more loosely organized nucleocapsid, rather than a helically symmetric coil. Nevertheless, this linear/helical core arrangement appears to be a general structural motif for the nidoviruses.

In either case, the non-isometric, linear arrangement of N does not present a uniform surface for the envelope proteins to interact with, consistent with the observed gap between the core and the envelope and the failure to detect substantial interactions between N and the endodomains of M and GP5 *in vitro* (unpublished data). In terms of the viral life cycle, this organization would obviate the need for disassembly of a closed shell-like core to release the genome into the cytoplasm after entry of the virus.

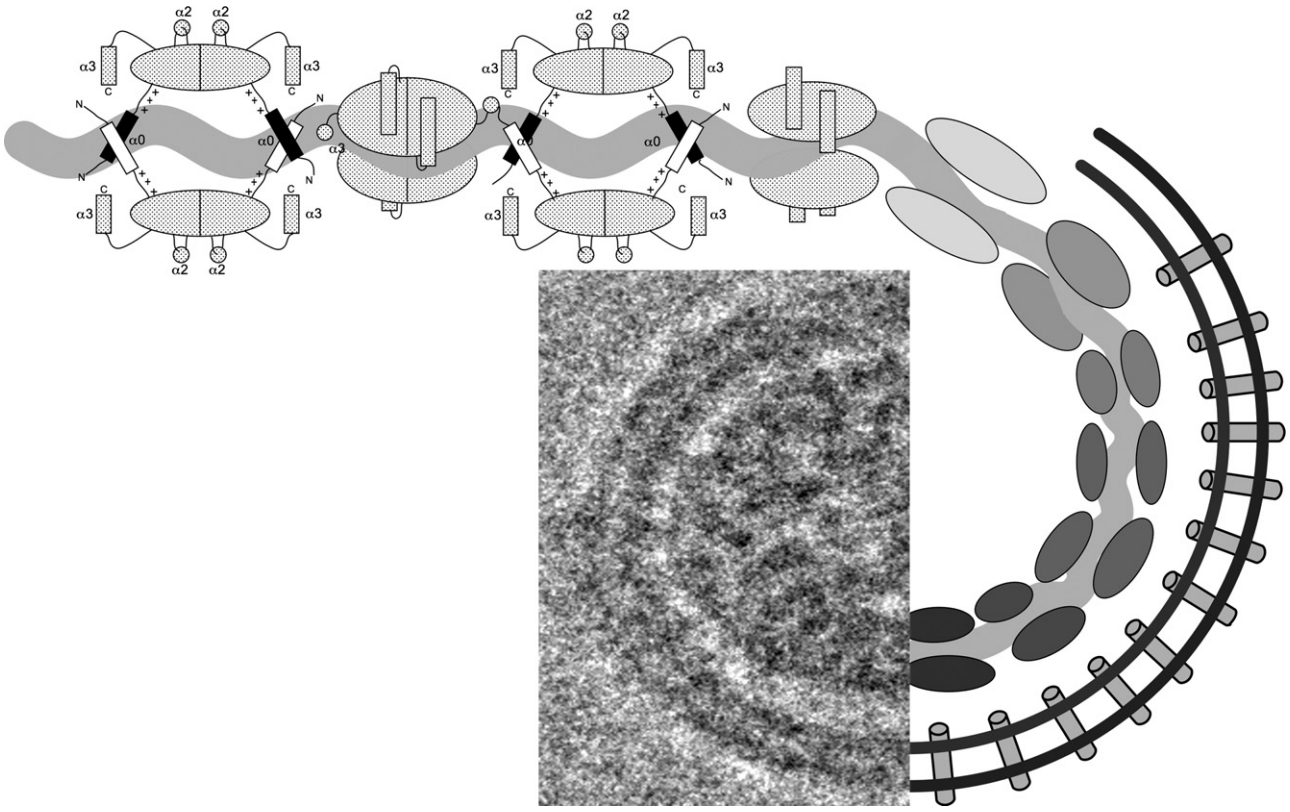

Fig. 7. Possible model for the nucleocapsid organization in the virion. The stippled oval shapes represent the N protein dimers. Pertinent structural features are indicated, including the α0, α2 and α3-helices and the positively charged N-terminal domains. These dimers are organized in a roughly helical fashion around the RNA (grey sinusoidal curve) through interactions with the N-terminal RNA-binding domains. This N–RNA ribbon is folded into the nucleocapsid, giving rise to the double-layered appearance of the viral core in electron micrographs, as shown. The "train track" represents the viral envelope with the TM domains of the major envelope proteins.

9. Perspectives

Although structural information on arteriviruses has lagged behind that of other enveloped (+) RNA viruses, our understanding of PRRSV structure has greatly increased in the last decade, leading to a better understanding of the viral life cycle, immunology and pathogenicity. One thing that has emerged from these studies is an appreciation of a close structural relationship between arteriviruses and other nidoviruses, in spite of large superficial differences.

There is clearly still much to do: PRRSV envelope protein structure is still a major unknown, in spite of the fact that these are arguably the most important proteins in the infection process, interactions with the host cells and the immune system. Currently, we know little of the nature of the envelope–host interactions, nor do we understand the fusion mechanism or the structural basis for immune evasion by PRRSV. A better understanding of PRRSV immunology, the mechanism of viral fusion and entry will be dependent on having detailed structural information on the envelope proteins. Further details on nucleocapsid assembly and genome packaging are also needed. The role of the many non-structural proteins in the viral replication process is also obscure.

Structural biology will continue to inform such studies and lead to a better understanding of the PRRSV properties that have made this pathogen such a problem to agriculture worldwide.

Acknowledgments

I would like to thank my co-workers and collaborators who have helped with various aspects of this project over the past several years, including Ashlesha A. Deshpande, Ying Fang, Eric A. Nelson, Cynthia M. Rodenburg, Jamil Saad, Michael S. Spilman, Craig Welbon and Dongwan Yoo. This work was in part supported by USDA grant 2006-01616.

References

Allaire, M., Chernala, M.M., Malcolm, B.A., James, M.N.G., 1994. Picornaviral 3C cysteine proteinases have a fold similar to chymotrypsin-like proteinases. Nature 369, 72–76.

Allende, R., Lewis, T.L., Lu, Z., Rock, D.L., Kutish, G.F., Ali, A., Doster, A.R., Osorio, F.A., 1999. North American and European porcine reproductive and respiratory syndrome viruses differ in non-structural protein coding regions. J. Gen. Virol. 80, 307–315.

Balasuriya, U.B., MacLachlan, N.J., 2004. The immune response to equine arteritis virus: potential lessons for other arteriviruses. Vet. Immunol. Immunopathol. 102, 107–129.

Barcena, M., Oostergetel, G.T., Bartelink, W., Faas, F.G.A., Verkleij, A., Rottier, P.J.M., Koster, A.J., Bosch, B.J., 2009. Cryo-electron tomography of mouse hepatitis virus: insights into the structure of the coronavirion. Proc. Natl. Acad. Sci. U.S.A. 106, 582–587.

Barrette-Ng, I.H., Ng, K.K.S., Mark, B.L., van Aken, D., Cherney, M.M., Garen, C., Kolodenko, Y., Gorbalenya, A.E., Snijder, E.J., James, M.N.G., 2002. Structure of arterivirus nsp4. J. Biol. Chem. 277, 39960–39966.

Batista, L., Pijoan, C., Dee, S., Olin, M., Molitor, T., Joo, H.S., XIao, Z., Murtaugh, M., 2004. Virological and immunological responses to porcine reproductive and respiratory syndrome virus in a large population of gilts. Can. J. Vet. Res. 68, 267–273.

Bautista, E.M., Faaberg, K.S., Mickelson, D., McGruder, E.D., 2002. Functional properties of the predicted helicase of porcine reproductive and respiratory syndrome virus. Virology 298, 258–270.

Benfield, D.A., Nelson, E., Collins, J.E., Harris, L., Goyal, S.M., Robison, D., Christianson, W.T., Morrison, R.B., Gorcyca, D., Chladek, D., 1992. Characterization of swine infertility and respiratory syndrome (SIRS) virus (isolate VR-2332). J. Vet. Diagn. Invest. 4, 127–133.

Blaha, T., 2000. The "colorful" epidemiology of PRRS. Vet. Res. 31, 77–83.

Brinton, M.A., 1994. Lactate dehydrogenase-elevating, equine arteritis and Lelystad viruses. In: Webster, R.G., Granoff, A. (Eds.), Encyclopedia of Virology, vol. 3. Academic Press, London, pp. 763–771.

Calvert, J.G., Slade, D.E., Shields, S.L., Jolie, R., Mannan, R.M., Ankenbauer, R.G., Welch, S.-K.W., 2007. CD163 expression confers susceptibility to porcine reproductive and respiratory syndrome viruses. J. Virol. 81, 7371–7379.
Cavanagh, D., 1997. Nidovirales: a new order comprising Coronaviridae and Arteriviridae. Arch. Virol. 142, 629–633.
Chang, C.K., Sue, S.C., Yu, T.H., Hsieh, C.M., Tsai, C.K., Chiang, Y.C., Lee, S.J., Hsiao, H.H., Wu, W.J., Chang, C.F., Huang, T.H., 2005. The dimer interface of the SARS coronavirus nucleocapsid protein adapts a porcine respiratory and reproductive syndrome virus-like structure. FEBS Lett. 579, 5563–5668.
Chen, C.-Y., Chang, C.-K., Chang, Y.-W., Sue, S.-C., Bai, H.-I., Riang, L., Hsiao, C.-D., Huang, T.-H., 2007. Structure of the SARS coronavirus nucleocapsid protein RNA-binding dimerization domain suggests a mechanism for helical packaging of viral RNA. J. Mol. Biol. 368, 1075–1086.
Choi, H.-K., Tong, L., Minor, W., Dumas, P., Boege, U., Rossmann, M.G., Wengler, G., 1991. Structure of Sindbis virus core protein reveals a chymotrypsin-like serine protease and the organization of the virion. Nature 354, 37–43.
Choi, H.K., Lu, G., Lee, S., Wengler, G., Rossmann, M.G., 1997. Structure of Semliki Forest virus core protein. Proteins 27, 345–359.
Conzelmann, K.K., Visser, N., Van Woensel, P., Thiel, H.J., 1993. Molecular characterization of porcine reproductive and respiratory syndrome virus, a member of the arterivirus group. Virology 193, 329–339.
Das, P.B., Dinh, P.X., Ansari, I.H., de Lima, M., Osorio, F.A., Pattnaik, A.K., 2010. The minor envelope glycoproteins GP2a and GP4 of porcine reproductive and respiratory syndrome virus interact with the receptor CD163. J. Virol. 84, 1731–1740.
Davies, H.A., Dourmashkin, R.R., Macnaughton, M.R., 1981. Ribonucleoprotein of avian infectious bronchitis virus. J. Gen. Virol. 53, 67–74.
de Lima, M., Ansari, I.H., Das, P.B., Ku, B.J., Martinez-Lobo, F.J., Pattnaik, A.K., Osorio, F.A., 2009. GP3 is a structural component of the PRRSV type II (US) virion. Virology 390, 31–36.
de Vries, A.A., Horzinek, M.C., Rottier, P.J.M., de Groot, R.J., 1997. The genome organization of the nidovirales: similarities and differences between arteri-, toro- and coronaviruses. Semin. Virol. 8, 33–47.
Dea, S., Gagnon, C.A., Mardassi, H., Pirzadeh, B., Rogan, D., 2000. Current knowledge on the structural proteins of porcine reproductive and respiratory syndrome (PRRS) virus: comparison of the North American and European isolates. Arch. Virol. 145, 659–688.
Dea, S., Sawyer, N., Alain, R., Athanassious, R., 1995. Ultrastructural characteristics and morphogenesis of porcine reproductive and respiratory syndrome virus propagated in the highly permissive MARC-145 cell clone. In: Talbot, P.J., Levy, G.A. (Eds.), Corona- and Related Viruses. Plenum Press, New York, pp. 95–98.
Delputte, P.L., Costers, S., Nauwynck, H.J., 2005. Analysis of porcine reproductive and respiratory syndrome virus attachment and internalization: distinctive roles for heparan sulfate and sialoadhesin. J. Gen. Virol. 86, 1441–1445.
Delputte, P.L., Nauwynck, H.J., 2004. Porcine arterivirus infection of alveolar macrophages is mediated by sialic acid on the virus. J. Virol. 78, 8094–8101.
Delputte, P.L., Van Breedam, W., Delrue, I., Oetke, C., Crocker, P.R., Nauwynck, H.J., 2007. Porcine arterivirus attachment to the macrophage-specific receptor sialoadhesin is dependent on the sialic acid-binding activity of the N-terminal immunoglobulin domain of sialoadhesin. J. Virol. 81, 9546–9550.
Delputte, P.L., Vanderheijden, N., Nauwynck, H.J., Paensaert, M.B., 2002. Involvement of the matrix protein in attachment of porcine reproductive and respiratory syndrome virus to a heparinlike receptor on porcine alveolar macrophages. J. Virol. 76, 4312–4320.
den Boon, J.A., Faaberg, K.S., Meulenberg, J.J., Wassenaar, A.L., Plagemann, P.G., Gorbalenya, A.E., 1995. Processing and evolution of the N-terminal region of the arterivirus replicase ORF1a protein: identification of two papainlike cysteine proteases. J. Virol. 69, 4500–4505.
Deshpande, A., Wang, S., Walsh, M.A., Dokland, T., 2007. Structure of the equine arteritis virus nucleocapsid protein reveals a dimer–dimer arrangement. Acta Crystallogr. D 63, 581–586.
Doan, D., Dokland, T., 2003. Structure of the nucleocapsid protein of porcine reproductive and respiratory syndrome virus. Structure 11, 1445–1451.
Dobbe, J.C., van der Meer, Y., Spaan, W.J.M., Snijder, E.J., 2001. Construction of chimeric arteriviruses reveals that the ectodomain of the major glycoprotein is not the main determinant of equine arterivirus tropism in cell culture. Virology 286, 283–294.
Dokland, T., Walsh, M., MacKenzie, J.M., Khromykh, A.A., Ee, K.-H., Wang, S., 2004. West Nile virus core protein: tetramer structure and ribbon formation. Structure 12, 1157–1163.
Duan, X., Nauwynck, H.J., Pensaert, M.B., 1997. Virus quantification and identification of cellular targets in the lungs and lymphoid tissues of pigs at different time intervals after inoculation with porcine reproductive and respiratory syndrome virus (PRRSV). Vet. Microbiol. 156, 9–19.
Fan, H., Ooi, A., Tan, Y.W., Wang, S., Fang, S., Liu, D.X., Lescar, J., 2005. The nucleocapsid protein of coronavirus infectious bronchitis virus: crystal structure of its N-terminal domain and multimerization properties. Structure 13, 1859–1868.
Fang, Y., Kim, D.-Y., Ropp, S., Steen, P., Christopher-Hennings, J., Nelson, E.A., Rowland, R.R.R., 2004. Heterogeity in Nsp2 of European-like porcine reproductive and respiratory syndrome viruses isolated in the United States. Virus Res. 100, 229–235.
Fang, Y., Schneider, P., Zhang, W.P., Faaberg, K.S., Nelson, E.A., Rowland, R.R.R., 2007. Diversity and evolution of a newly emerged North American Type 1 porcine arterivirus: analysis of isolates collected between 1999 and 2004. Arch. Virol. 152, 1009–1017.
Forsberg, R., 2005. Divergence time of porcine reproductive and respiratory syndrome virus subtypes. Mol. Biol. Evol. 22, 2131–2134.
Frias-Staheli, N., Giannakopolous, N.V., Kikkert, M., Taylor, S.L., Bridgen, A., Paragas, J., Richt, J.A., Rowland, R.R., Schmaljohn, C.S., Lenschow, D.J., Snijder, E.J., Garcia-Sastre, A., Virgin, H.W., 2007. Ovarian tumor domain-containing viral proteases evade ubiquitin- and ISG15-dependent innate immune responses. Cell Host Microbe 2, 404–416.
Gao, Z.Q., Guo, X., Yang, H.C., 2004. Genomic characterization of two Chinese isolates of porcine respiratory and reproductive syndrome virus. Arch. Virol. 149, 1341–1351.
Gonin, P., Mardassi, H., Gagnon, C.A., Massie, B., Dea, S., 1998. A nonstructural and antigenic glycoprotein is encoded by ORF3 of the IAF-Klop strain of porcine reproductive and respiratory syndrome virus. Arch. Virol. 143, 1927–1940.
Gonin, P., Pirzadeh, B., Gagnon, C.A., Dea, S., 1999. Seroneutralization of porcine reproductive and respiratory syndrome virus correlates with antibody response to the GP5 major envelope glycoprotein. J. Vet. Diagn. Invest. 11, 20–26.
Gonzalez, M.E., Carrasco, L., 2003. Viroporins. FEBS Lett. 552, 28–34.
Gorbalenya, A.E., Enjuanes, L., Ziebuhr, J., Snijder, E.J., 2006. Nidovirales: evolving the largest RNA virus genome. Virus Res. 117, 17–37.
Guarne, A., Tormo, J., Kirchweger, R., Pfistermueller, D., Fita, I., Skern, T., 1998. Structure of the foot-and-mouth disease virus leader protease: a papain-like fold adapted for self-processing and eIF4G recognition. EMBO J. 17, 7469–7479.
Han, J., Rutherford, M.S., Faaberg, K.S., 2009. The porcine reproductive and respiratory syndrome virus nsp2 cysteine protease domain possesses both trans- and cis-cleavage activities. J. Virol. 83, 9449–9463.
Harris, A., Cardone, G., Winkler, D.C., Heymann, J.B., Brecher, M., White, J.M., Steven, A.C., 2006. Influenza virus pleiomorphy characterized by cryoelectron tomography. Proc. Natl. Acad. Sci. U.S.A. 103, 19123–19127.
Harrison, S.C., 2008. Viral membrane fusion. Nat. Struct. Mol. Biol. 15, 690–698.
Holmes, K.V., Lai, M.M.C., 1996. Coronaviridae: the viruses and their replication. In: Fields, B.N., Knipe, D.M., Howley, P.M. (Eds.), Fundamental Virology, 3rd ed. Lippincott-Raven Publishers, Philadelphia.
Horzinek, M.C., 1981. Non-arthropod borne togaviruses. In: Tinsley, T.W., Brown, F. (Eds.), Experimental Virology. Academic Press, London.
Huang, Q., Yu, L., Petros, A.M., Gunasekera, A., Liu, Z., Xu, N., Hajduk, P., Mack, J., Fesik, S.W., Olejniczak, E.T., 2004. Structure of the N-terminal RNA-binding domain of the SARS CoV nucleocapsid protein. Biochemistry 43, 6059–6063.
Jayaram, H., Fan, H., Bowman, B.R., Ooi, A., Jayaram, J., Collisson, E.W., Lescar, J., Prasad, B.V.V., 2006. X-ray structures of the N- and C-terminal domains of a coronavirus nucleocapsid protein: implications for nucleocapsid formation. J. Virol. 80, 6612–6620.
Kapur, V., Elam, M.R., Pawlovich, T.M., Murtaugh, M.P., 1996. Genetic variation in porcine reproductive and respiratory syndrome virus isolates in the midwestern United States. J. Gen. Virol. 77, 1271–1276.
Kim, H.S., Kwang, J., Yoon, I.J., Joo, H.S., Frey, M.L., 1993. Enhanced replication of procine reproductive and respiratory syndrome (PRRS) virus in a homogeneous subpopulation of MA-104 cell line. Arch. Virol. 133, 477–483.
Kreutz, L.C., 1998. Cellular membrane factors are the major determinants of porcine reproductive and respiratory syndrome virus tropism. Virus Res. 53, 121–128.
Kroese, M.V., Zevenhoven-Dobbe, J.C., Bos-de Ruijter, J.N., Peeters, B.P., Meulenberg, J.J., Cornelissen, L.A., Snijder, E.J., 2008. The nsp1alpha and nsp1 papain-like autoproteinases are essential for porcine reproductive and respiratory syndrome virus RNA synthesis. J. Gen. Virol. 89, 494–499.
Lee, C., Yoo, D., 2006. The small envelope protein of porcine reproductive and respiratory syndrome virus possesses ion channel protein-like properties. Virology 355, 30–43.
Lee, Y.J., Park, C.-K., Nam, E., Kim, S.H., Lee, O.-S., Lee, D.S., Lee, C., 2010. Generation of a porcine alveolar macrophage cell line for the growth of porcine reproductive and respiratory syndrome virus. J. Virol. Methods 163, 410–415.
Lucic, V., Forster, F., Baumeister, W., 2005. Structural studies by electron tomography: from cells to molecules. Annu. Rev. Biochem. 74, 833–865.
Mardassi, H., Athanassious, R., Mounir, S., Dea, S., 1994. Porcine reproductive and respiratory syndrome virus: morphological, biochemical and serological characteristics of Quebec isolates associated with acute and chronic outbreaks of porcine reproductive and respiratory syndrome. Can. J. Vet. Res. 58, 55–64.
Mardassi, H., Gonin, P., Gagnon, C.A., Massie, B., Dea, S., 1998. A subset of porcine reproductive and respiratory syndrome virus GP3 glycoprotein is released into the culture medium of cells as a non-virion-associated and membrane-free (soluble) form. J. Virol. 72, 6298–6306.
Mardassi, H., Massie, B., Dea, S., 1996. Intracellular synthesis, processing and transport of proteins encoded by ORFs 5 to 7 of porcine reproductive and respiratory syndrome virus. Virology 221, 98–112.
Melton, J.V., Ewart, G.D., Weir, R.C., Board, P.G., Lee, E., Gage, P.W., 2002. Alphavirus 6K proteins form ion channels. J. Biol. Chem. 277, 46923–46931.
Meng, X.J., 2000. Heterogeneity of porcine reproductive and respiratory syndrome virus: implications for current vaccine efficacy and future vaccine development. Vet. Microbiol. 12, 309–329.
Meng, X.J., Paul, P.S., Halbur, P.G., Lum, M.A., 1995a. Phylogenetic analyses of the putative M (ORF6) and N (ORF7) genes of porcine reproductive and respiratory syndrome virus (PRRSV): implication for the existence of two genotypes of PRRSV in the U.S.A. and Europe. Arch. Virol. 140, 745–755.
Meng, X.J., Paul, P.S., Halbur, P.G., Morozov, I., 1995b. Sequence comparison of open reading frames 2 to 5 of low and high virulence United States isolates of porcine reproductive and respiratory syndrome virus. J. Gen. Virol. 76, 3181–3188.
Meulenberg, J.J., Bende, R.J., Pol, J.M., Wenswoort, G., Moormann, R.J., 1995a. Nucleocapsid protein N of Lelystad virus: expression by recombinant baculovirus, immunological properties, and suitability for detection of serum antibodies. Clin. Diagn. Lab. Immunol. 2, 652–656.

Meulenberg, J.J., Hulst, M.M., de Meijer, E.J., Moonen, P.L., den Besten, A., de Kluyver, E.P., Wenswoort, G., Moormann, R.J., 1993. Lelystad virus, the causative agent of porcine epidemic abortion and respiratory syndrome (PEARS), is related to LDV and EAV. Virology 192, 62–72.

Meulenberg, J.J., Petersen-den Besten, A., De Kluyverer, E.P., Moormann, R.J., Schaaper, W.M., Wenswoort, G., 1995b. Characterization of proteins encoded by ORFs 2 to 7 of Lelystad virus. Virology 206, 155–163.

Meulenberg, J.J., van Nieuwstadt, A.P., van Essen-Zandbergen, A., Langeveld, J.P., 1997. Posttranslational processing and identification of a neutralization domain of the GP4 protein encoded by ORF4 of Lelystad virus. J. Virol. 71, 6061–6067.

Misinzo, G.M., Delputte, P.L., Nauwynck, H.J., 2008. Involvement of proteases in porcine reproductive and respiratory syndrome virus uncoating upon internalization in primary macrophages. Vet. Res. 39, 55.

Molenkamp, R., van Tol, H., Rozier, B.C., van der Meer, Y., Spaan, W.J.M., Snijder, E.J., 2000. The arterivirus replicase is the only viral protein required for genome replication and subgenomic mRNA transcription. J. Gen. Virol. 81, 2491–2496.

Murtaugh, M.P., Elam, M.R., Kakach, L.T., 1995. Comparison of the structural protein coding sequences of the VR-2332 and Lelystad virus strains of the PRRS virus. Arch. Virol. 140, 1451–1460.

Murtaugh, M.P., Xiao, Z., Zuckermann, F., 2002. Immunological responses of swine to porcine reproductive and respiratory syndrome virus infection. Viral Immunol. 15, 533–547.

Nam, E., Park, C.K., Kim, S.H., Joo, Y.S., Yeo, S.G., Lee, C., 2009. Complete genomic characterization of a European type 1 porcine reproductive and respiratory syndrom virus isolate in Korea. Arch. Virol. 154, 629–638.

Nedialkova, D.D., Ulferts, R., van den Born, E., Lauber, C., Gorbalenya, A.E., Ziebuhr, J., Snijder, E.J., 2009. Biochemical characterization of arterivirus nonstructural protein 11 reveals the nidovirus-wide conservation of a replicative endoribonuclease. J. Virol. 83, 5671–5682.

Nelsen, C.J., Murtaugh, M.P., Faaberg, K.S., 1999. Porcine reproductive and respiratory syndrome virus comparison: divergent evolution on two continents. J. Virol. 73, 270–280.

Neuman, B.W., Adair, B.D., Yoshioka, C., Quispe, J.D., Milligan, R.A., Yeager, M., Buchmeier, M.J., 2006a. Ultrastructure of SARS-CoV, FIPV, and MHV revealed by electron cryomicroscopy. Adv. Exp. Med. Biol..

Neuman, B.W., Adair, B.D., Yoshioka, C., Quispe, J.D., Orca, G., Kuhn, P., Milligan, R.A., Yeager, M., Buchmeier, M.J., 2006b. Supramolecular architecture of severe acute respiratory syndrome coronavirus revealed by electron cryomicroscopy. J. Virol. 80, 7918–7928.

Ostrowski, M., Galeota, J.A., Jar, A.M., Platt, K.B., Osorio, F.A., Lopez, O.J., 2002. Identification of neutralizing and nonneutralizing epitopes in the porcine reproductive and respiratory syndrome virus GP5 ectodomain. J. Virol. 76, 4242–4250.

Owen, K.E., Kuhn, R.J., 1997. Alphavirus budding is dependent on the interaction between the nucleocapsid and hydrophobic amino acids on the cytoplasmic domain of the E2 envelope glycoprotein. Virology 230, 187–196.

Pedersen, K.W., van der Meer, Y., Roos, N., Snijder, E.J., 1999. Open reading frame 1a-encoded subunits of the arterivirus replicase induce endoplasmic reticulum-derived double-membrane vesicles which carry the viral replication complex. J. Virol. 73, 2016–2026.

Perera, R., Owen, K.E., Tellinghuisen, T.L., Gorbalenya, A.E., Kuhn, R.J., 2001. Alphavirus nucleocapsid protein contains a putative coiled coil alpha-helix important for core assembly. J. Virol. 75, 1–10.

Pettersen, E.F., Goddard, T.D., Huang, C.C., Couch, G.S., Greenblatt, D.M., Meng, E.C., Ferrin, T.E., 2004. UCSF Chimera – a visualization system for exploratory research and analysis. J. Comput. Chem. 25, 1605–1612.

Pinto, L.H., Holsinger, L.J., Lamb, R.A., 1992. Influenza virus M2 protein has ion channel activity. Cell 69, 517–528.

Pirzadeh, B., Dea, S., 1997. Monoclonal antibodies to the ORF5 product of porcine reproductive and respiratory syndrome virus define linear neutralizing determinants. J. Gen. Virol. 78, 1867–1873.

Plagemann, P.G.W., Moennig, V., 1992. Lactate dehydrogenase-elevating virus, equine arteritis virus, and simian hemorrhagic fever virus, a new group of positive-strand RNA viruses. Adv. Virus Res. 41, 99–192.

Posthuma, C.C., Pedersen, K.W., Lu, Z., Joosten, R.G., Roos, N., Zevenhoven-Dobbe, J.C., Snijder, E.J., 2008. Formation of the arterivirus replication/transcription complex: a key role for nonstructural protein 3 in the remodeling of intracellular membranes. J. Virol. 82, 4480–4491.

Qiu, Z., Hingley, S.T., Simmons, G., Yu, C., Das Sarma, J., Bates, P., Weiss, S.R., 2006. Endosomal proteolysis by cathepsins is necessar for murine coronavirus mouse hepatitis virus type 2 spike-mediated entry. J. Virol. 80, 5768–5776.

Ratia, K., Saikatendu, K.S., Santarsiero, B.D., Barretto, N., Baker, S.C., Stevens, R.C., Mesecar, A.D., 2006. Severe acute respiratory syndrome coronavirus papain-like protease: structure of a viral deubiquitinating enzyme. Proc. Natl. Acad. Sci. U.S.A. 103, 5717–5722.

Ropp, S.L., Wees, C.E.M., Fang, Y., Nelson, E.A., Rossow, K.D., Bien, M., Arndt, B., Preszler, S., Steen, P., Christopher-Hennings, J., Collins, J.E., Benfield, D.A., Faaberg, K.S., 2004. Characterization of emerging European-like porcine reproductive and respiratory syndrome virus isolates in the United States. J. Virol. 78, 3684–3703.

Rossow, K.D., 1998. Porcine reproductive and respiratory syndrome. Vet. Pathol. 35, 1–20.

Rowland, R.R., Schneider, P., Fang, Y., Wootton, S., Yoo, D., Benfield, D.A., 2003. Peptide domains involved in the localization of the porcine reproductive and respiratory syndrome virus nucleocapsid protein to the nucleolus. Virology 316, 135–145.

Saper, M.A., Bjorkman, P.J., Wiley, D.C., 1991. Refined structure of the human histocompatibility antigen HLA-A2 at 2.6 Å resolution. J. Mol. Biol. 219, 277–319.

Seybert, A., Posthuma, C.C., van Dinten, L.C., Snijder, E.J., Gorbalenya, A.E., Ziebuhr, J., 2005. A complex zinc finger controls the enzymatic activities of nidovirus helicases. J. Virol. 79, 696–704.

Seybert, A., van Dinten, L.C., Snijder, E.J., Ziebuhr, J., 2000. Biochemical characterization of the equine arteritis virus helicase suggests a close functional relationship between arterivirus and coronavirus helicases. J. Virol. 74, 9586–9593.

Simmons, G., Gosalia, D.N., Rennekamp, A.J., Reeves, J.D., Diamond, S.L., Bates, P., 2005. Inhibitors of cathepsin L prevent severe acute respiratory syndrome coronavirus entry. Proc. Natl. Acad. Sci. U.S.A. 102, 11876–11881.

Snijder, E.J., Horzinek, M.C., Spaan, W.J.M., 1993. The coronaviruslike superfamily. Adv. Exp. Med. Biol. 342, 235–244.

Snijder, E.J., Meulenberg, J.J.M., 1998. The molecular biology of arteriviruses. J. Gen. Virol. 79, 961–979.

Snijder, E.J., van Tol, H., Pedersen, K.W., Raamsman, M.J., de Vries, A.A.F., 1999. Identification of a novel structural protein of arteriviruses. J. Virol. 73, 6335–6345.

Snijder, E.J., van Tol, H., Roos, N., Pedersen, K.W., 2001. Non-structural proteins 2 and 3 interact to modify host cell membranes during the formation of the arterivirus replication complex. J. Gen. Virol. 82, 985–994.

Snijder, E.J., Wassenaar, A.L.M., van Dinten, L.C., Spaan, W.J.M., Gorbalenya, A.E., 1995. The arterivirus NSP2 protease: an unusual cysteine protease with primary structure similarities to both papain-like and chymotrypsin-like proteases. J. Biol. Chem. 270, 16671–16676.

Snijder, E.J., Wassenaar, A.L.M., van Dinten, L.C., Spaan, W.J.M., Gorbalenya, A.E., 1996. The arterivirus Nsp4 protease is the prototype of a novel group of chymotrypsin-like proteases, the 3C-like serine proteases. J. Biol. Chem. 271, 4864–4871.

Song, C., Lu, R., Bienzle, D., Liu, H.C., Yoo, D., 2009. Interaction of the porcine reproductive and respiratory syndrome virus nucleocapsid protein with the inhibitor of MyoD family-a domain-containing protein. Biol. Chem. 390, 215–223.

Spilman, M.S., Welbon, C., Nelson, E., Dokland, T., 2009. Cryo-electron tomography of porcine reproductive and respiratory syndrome virus: organization of the nucleocapsid. J. Gen. Virol. 90, 527–535.

Stadejek, T., Stankevicius, A., Storgaard, T., Oleksiewicz, M.B., Belak, S., Drew, T.W., Pejsak, Z., 2002. Identification of radically different variants of porcine reproductive and respiratory syndrome virus in Eastern Europe: towards a common ancestor for European and American viruses. J. Gen. Virol. 83, 1861–1873.

Strauss, J.H., Strauss, E.G., 2002. Viruses and Human Disease. Academic Press, San Diego.

Sturman, L.S., Holmes, K.V., Behnke, J., 1980. Isolation of coronavirus envelope glycoproteins and interaction with the viral nucleocapsid. J. Virol. 33, 449–462.

Subramaniam, S., 2005. Bridging the imaging gap: visualizing subcellular architecture with electron tomography. Curr. Opin. Microbiol. 8, 316–322.

Sun, Y., Xue, F., Guo, Y., Ma, M., Hao, N., Zhang, X.J., Lou, Z., Li, X., Rao, Z., 2009. Crystal structure of porcine reproductive and respiratory syndrome virus leader protease NSP1alpha. J. Virol. 83, 10931–10940.

Tian, X., Lu, G., Gao, F., Peng, H., Feng, Y., Ma, G., Bartlam, M., Tian, K., Yan, J., Hilgenfeld, R., Gao, G.F., 2009. Structure and cleavage specificity of the chymotrypsin-like serine protease (3CLSP/nsp4) of porcine reproductive and respiratory syndrome virus (PRRSV). J. Mol. Biol. 392, 977–993.

Tijms, M.A., Nedialkova, D.D., Zevenhoven-Dobbe, J.C., Gorbalenya, A.E., Snijder, E.J., 2007. Arterivirus subgenomic mRNA synthesis and virion biogenesis depend on the multifunctional nsp1 autoprotease. J. Virol. 81, 10496–10505.

Tijms, M.A., Snijder, E.J., 2003. Equine arteritis virus non-structural protein 1, an essential factor for viral subgenomic mRNA synthesis, interacts with the cellular transcription co-factor p100. J. Gen. Virol. 84, 2317–2322.

Tijms, M.A., van Dinten, L.C., Gorbalenya, A.E., Snijder, E.J., 2001. A zinc finger-containing papain-like protease couples subgenomic mRNA synthesis to genome translation in a positive-stranded RNA virus. Proc. Natl. Acad. Sci. U.S.A. 98, 1889–1894.

Valegård, K., Liljas, L., Fridborg, K., Unge, T., 1990. The three-dimensional structure of the bacterial virus MS2. Nature (London) 345, 36–41.

van Aken, D., Zevenhoven-Dobbe, J.C., Gorbalenya, A.E., Snijder, E.J., 2006. Proteolytic maturation of replicase polyprotein pp1a by the nsp4 main proteinase is essential for equine arteritis virus replication and includes internal cleavage of nsp7. J. Gen. Virol. 87, 3473–3482.

Van Breedam, W., Van Gorp, H., Zhang, J.Q., Crocker, P.R., Delputte, P.L., Nauwynck, H.J., 2010. The M/GP5 glycoprotein complex of porcine reproductive and respiratory syndrome virus binds the sialoadhesin receptor in a sialic acid-dependent manner. PLoS Pathog. 6, e1000730.

van Dinten, L.C., Rensen, S., Gorbalenya, A.E., Snijder, E.J., 1999. Proteolytic processing of the open reading frame 1b-encoded part of arterivirus replicase is mediated by nsp4 serine protease and is essential for virus replication. J. Virol. 73, 2027–2037.

van Dinten, L.C., Wassenaar, A.L.M., Gorbalenya, A.E., Spaan, W.J.M., Snijder, E.J., 1996. Processing of the equine arteritis virus replicase ORF1b protein: identification of cleavage products containing the putative viral polymerase and helicase domains. J. Virol. 70, 6625–6633.

Van Gorp, H., Van Breedam, W., Delputte, P.L., Nauwynck, H.J., 2008. Sialoadhesin and CD163 join forces during entry of the porcine reproductive and respiratory syndrome virus. J. Gen. Virol. 89, 2943–2953.

van Nieuwstadt, A.P., Meulenberg, J.J., van Essen-Zandbergen, A., Petersen-den Besten, A., Bende, R.J., Moormann, R.J., Wenswoort, G., 1996. Proteins encoded by open reading frames 3 and 4 of the genome of Lelystad virus (Arteriviridae) are structural proteins of the virion. J. Virol. 70, 4767–4772.

Vanderheijden, N., Delputte, P.L., Favoreel, H.W., Vandekerckhove, J., Van Damme, J., van Woensel, P.A., Nauwynck, H.J., 2003. Involvement of sialoadhesin in entry

of porcine reproductive and respiratory syndrom virus into porcine alveolar macrophages. J. Virol. 77, 8207–8215.
Verheije, M.H., Welting, T.J., Jansen, H.T., Rottier, P.J.M., Meulenberg, J.J., 2002. Chimeric arteriviruses generated by swapping of the M protein ectodomain rule out a role of this domain in viral targeting. Virology 303, 364–373.
Weiland, E., Wieczorek-Krohmer, M., Kohl, D., Conzelmann, K.K., Weiland, F., 1999. Monoclonal antibodies to the GP5 of porcine reproductive and respiratory syndrome virus are more effective in virus neutralization than monoclonal antibodies to the GP4. Vet. Microbiol. 66, 171–186.
Wierenga, R., de Vries, A.A., Raamsman, M.J., Rottier, P.J.M., 2002. Characterization of two new structural glycoproteins, GP3 and GP4, of equine arteritis virus. J. Virol. 76, 10829–10840.
Wieringa, R., de Vries, A.A., Rottier, P.J.M., 2003a. Formation of disulfide-linked complexes between the three minor envelope glycoproteins (GP2b, GP3 and GP4) of equine arteritis virus. J. Virol. 77, 6216–6226.
Wieringa, R., de Vries, A.A., van der Meulen, J., Godeke, G.J., Onderwater, J.J., van Tol, H., Koerten, H.K., Mommaas, A.M., Snijder, E.J., Rottier, P.J.M., 2004. Structural protein requirements in equine arteritis virus assembly. J. Virol. 78, 13019–13027.
Wieringa, R., de Vries, A.A.F., Post, S.M., Rottier, P.J.M., 2003b. Intra- and intermolecular disulfide bonds of the GP2b glycoprotein of equine arteritis virus: relevance for virus assembly and infectivity. J. Virol. 77, 12996–13004.
Wissink, E.H.J., Kroese, M.V., Maneschijn-Bonsing, J.G., Meulenberg, J.J.M., van Rijn, P.A., Rijsewijk, F.A.M., Rottier, P.J.M., 2004. Significance of the oligosaccharides of the porcine reproductive and respiratory syndrome virus glycoproteins GP2a and GP5 for infectious virus production. J. Gen. Virol. 85, 3715–3723.
Wissink, E.H.J., Kroese, M.V., van Wijk, H.A.R., Rijsewijk, F.A.M., Meulenberg, J.J., Rottier, P.J.M., 2005. Envelope protein requirements for the assembly of infectious virions or porcine reproductive and respiratory syndrome virus. J. Virol. 79, 12495–12506.
Wissink, E.H.J., van Wijk, H.A.R., Kroese, M.V., Weiland, E., Meulenberg, J.J., Rottier, P.J.M., van Rijn, P.A., 2003. The major envelope protein, GP5, of a European porcine reproductive and respiratory syndrome virus contains a neutralization epitope in its N-terminal ectodomain. J. Gen. Virol. 84, 1535–1543.
Wootton, S., Yoo, D., 2003. Homo-oligomerization of the porcine reproductive and respiratory syndrome virus nucleocapsid protein and the role of disulfide linkages. J. Virol. 77, 4546–4557.
Wootton, S.K., Rowland, R.R., Yoo, D., 2002. Phosphorylation of the porcine reproductive and respiratory syndrome virus nucleocapsid protein. J. Virol. 76, 10569–10576.
Wu, W.H., Fang, Y., Farwell, R., Steffen-Bien, M., Rowland, R.R., Christopher-Hennings, J., Nelson, E.A., 2001. A 10-kDa structural protein of porcine reproductive and respiratory syndrome virus encoded by ORF2b. Virology 287, 183–191.
Wu, W.H., Fang, Y., Rowland, R.R., Lawson, S.R., Christopher-Hennings, J., Yoon, K.J., Nelson, E.A., 2005. The 2b protein as a minor structural component of PRRSV. Virus Res. 114, 177–181.
Xue, F., Sun, Y., Yan, L., Zhao, C., Chen, J., Bartlam, M., Li, X., Lou, Z., Rao, Z., 2010. The crystal structure of porcine reproductive and respiratory syndrome virus nonstructural protein Nsp1beta reveals a novel metal-dependent nuclease. J. Virol. 84, 6461–6471.
Yang, L., Frey, M.L., Yoon, K.J., Zimmermann, J.J., Platt, K.B., 2000. Categorization of North American porcine reproductive and respiratory syndrome viruses: epitopic profiles of the N, M, GP5 and GP3 proteins and susceptibility to neutralization. Arch. Virol. 145, 1599–1619.
Yoo, D., Wootton, S., Li, G., Song, S., Rowland, R.R., 2003. Colocalization and interaction of the porcine arterivirus nucleocapsid protein with the small nucleolar RNA-associated protein fibrillarin. J. Virol. 77, 12173–12183.
Yu, I.M., Oldham, M.L., Zhang, J., Chen, J., 2006. Crystal structure of the severe acute respiratory syndrome (SARS) coronavirus nucleocapsid protein dimerization domain reveals evolutionary linkage between corona- and arteriviridae. J. Biol. Chem. 281, 17134–17139.
Ziebuhr, J., Snijder, E.J., Gorbalenya, A.E., 2000. Virus-encoded proteinases and proteolytic processing in the Nidovirales. J. Gen. Virol. 81, 853–879.
Zimmerman, J.J., Yoon, K.J., Wills, R.W., Swenson, S.L., 1997. General overview of PRRSV: a perspective from the United States. Vet. Microbiol. 55, 187–196.